Metallocene Copolymers of Propene and 1-Hexene: The Influence of the Comonomer Content and Thermal History on the Structure and Mechanical Properties

J. M. LÓPEZ-MAJADA,[1] H. PALZA,[2,3] J. L. GUEVARA,[2–4] R. QUIJADA,[2,3] M. C. MARTÍNEZ,[5] R. BENAVENTE,[1] J. M. PEREÑA,[1] E. PÉREZ,[1] M. L. CERRADA[1]

[1]Instituto de Ciencia y Tecnología de Polímeros, Juan de la Cierva 3, 28006 Madrid, Spain

[2]Departamento de Ingeniería Química, Facultad de Ciencias Físicas y Matemáticas, Universidad de Chile, Casilla 2777

[3]Centro para la Investigación Multidisciplinaria Avanzada en Ciencias de los Materiales, Santiago, Chile

[4]Departamento de Química, Universidad Católica del Norte, Avenida Angamos 0610, Antofagasta, Chile

[5]CTR Repsol-YPF, Móstoles, Madrid, Spain

ABSTRACT: The relationships between the structure and properties have been established for copolymers of propylene and 1-hexene synthesized with an isotactic metallocene catalyst system. The most important factor affecting the structure and properties of these copolymers is the comonomer content. The thermal treatment, that is, the rate of cooling from the melt, is also important. These factors affect the thermal properties, the degree of crystallinity, and therefore the structural parameters and the viscoelastic behavior. A slow cooling from the melt favors the formation of the γ phase instead of the α modification. Regarding the viscoelastic behavior, the β relaxation, associated with the glass-transition temperature, is shifted to lower temperatures and its intensity is increased as the 1-hexene content raises. The microhardness values are correlated with those of the storage modulus deduced from dynamic mechanical thermal analysis curves, and good linear relations have been obtained between these parameters.

Keywords: α and γ forms; isotactic polypropylene; metallocene catalysts; propylene–1-hexene copolymers; SAXS

INTRODUCTION

Isotactic polypropylene (iPP) is one of the thermoplastic polymers primarily used in industry and has bigger growth inside commodity polymers because it presents interesting behavior: good environmental resistance, the possibility of being processed by different methods (extrusion, injection, and blow molding), and ease of recycling at a moderate cost. Moreover, iPP exhibits a lower density than other polymers such as high-density polyethylene (HDPE; 5%), polystyrene (PS; 14%), and poly (ethylene terephthalate) (PET; 50%). This feature is really important for its extensive use and production all over the world because any object manufactured with iPP requires less material than the same object made with some other polymers.[1]

Correspondence to: M. L. Cerrada (E-mail: mlcerrada@ictp.csic.es)

However, one of the inconveniences of iPP is its insufficient impact strength at low environmental temperatures near its glass-transition temperature. The glass-transition temperature of iPP is about 0 °C, depending on variables such as the crystallinity, crystal morphology, molecular weight, and level of isotacticity. To provide an enhancement of the impact properties of iPP, its blending with various types of elastomers has gained much attention in recent years because of its great industrial and commercial importance. Additionally, polypropylene (PP) has also been blended with different polyethylenes (HDPE, low-density polyethylene, and linear low-density polyethylene). However, the problem with these blends is the formation of incompatible phases and interphases. Consequently, the use of compatibilizing agents is necessary to attain an optimum blend and really improve the impact resistance. One possibility for overcoming the difficulties of the miscibility of the different polymer phases is reactor granule technology, which leads to heterophasic copolymers[2] with an excellent stiffness/impact balance[3,4] and a wide range of ethylene contents (up to 25 wt %) as the rubber phase.

On the other hand, the polymerization and copolymerization of polyolefins have undergone great advances with the discovery of metallocene catalysts by Kaminsky and coworkers[5–7] because of their great versatility. Concerning propene homopolymerization, the use of these catalytic systems has allowed the synthesis of PP with several tacticities (isotactic, atactic, syndiotactic, hemiisotactic, etc.), with only the structure of the catalyst being changed.[8,9] Moreover, these metallocene catalysts allow the incorporation of rubbery polyolefinic macromonomers, such as atactic polypropene[10] and poly(ethylene-*co*-propylene),[11–13] into macromolecules, making feasible the coexistence of hard and soft segments within the chains. These novel copolymers constitute a very interesting approach to stiffness/impact resistance optimization.

Another alternative for modifying the iPP structure and, therefore, its properties without the necessity of blending it with other polymers is the copolymerization of propene with α-olefins of different chain lengths.[14–16] The interest in these copolymers is twofold: first, they might improve the final behavior of iPP, and second, these new materials obtained by this synthetic route might exhibit interesting novel properties. In contrast to the previously mentioned approach, the development of soft and hard domains, this methodology primarily changes the iPP crystalline structure, and so a good rigidity/toughness balance and better transparency can be attained at a given optimum comonomer content.

The thermal treatment applied to polymers is important because the structure and mechanical properties strongly depend on the thermal history imposed during processing. In particular, iPP can crystallize into different crystalline structures according to the crystallization conditions.[17] The development of the α, β, γ, or smectic forms depends on the crystallization conditions[18,19] and on the number of structural irregularities of the polymeric chain.[20]

The most typical and most stable crystalline structure, the monoclinic α form, was characterized for the first time by Natta and Corradini.[21] The hexagonal β modification appears only under special crystallization conditions or in the presence of selective β nucleating agents. The orthorhombic γ form has been found in the case of low-molecular-weight iPP[17,22,23] and in random copolymers of propylene and α-olefins, favored when the proportion of the incorporated comonomer is increased.[24] Moreover, the γ modification is especially favored in the case of iPP synthesized by metallocene catalysts because of the presence of errors homogeneously distributed among the different polymer chains.[25]

The objective of this work was to study the effects of the incorporation of 1-hexene and the thermal treatment on the final properties of propylene–1-hexene copolymers synthesized by a metallocene catalyst. The structural and thermal characterization was carried out by X-ray diffraction (profiles at wide and small angles) and calorimetric analyses, whereas the evaluation of the mechanical behavior was performed by dynamic mechanical thermal analysis and microhardness (MH) determination.

EXPERIMENTAL

Polymerization

Two copolymers of propene and 1-hexene were prepared with an isotactic metallocene catalyst for the direct copolymerization.[15,26] The reactions were carried out at 55 °C and 2 bar of pressure of propene, with a relation cocatalyst/catalyst (Al/Zr) of 1000, within a 1-L Büchi autoclave reactor for 30 min, in a process-type slurry with toluene as the solvent. For all the reactions, 5.0×10^{-6} mol

of the catalyst *rac*-Et(2-Me–Ind)$_2$ZrCl$_2$ was used, and methylaluminoxane was employed as the cocatalyst. The initial concentrations of the comonomer in the feed were 0.13 and 0.32 mol/L, respectively, for the two copolymers, and the solvent volume was adjusted in such a way that the total volume inside the reactor was 500 mL. An iPP homopolymer sample was prepared under the same conditions for comparative reasons.

Characterization

The comonomer (1-hexene) content and the tacticity (% mm) of the samples, determined by ^{13}C NMR spectroscopy, are shown in Table 1. ^{13}C NMR spectra of the samples were recorded with a Varian Inova 300 spectrometer operating at 75 MHz and at 90 °C. The samples were dissolved in *o*-dichlorobenzene, and benzene-d_6 (20% v/v) was used for the internal lock in a 5-mm NMR probe. The experimental parameters were as follows: an acquisition time of 1.5 s, a relaxation time of 4.0 s, and a pulse angle of 74°.

The molecular weights were determined by gel permeation chromatography (GPC) in a Waters Alliance 2000 chromatograph equipped with a differential refractive-index detector and a set of three columns.[15] The columns were calibrated with monodisperse PS standards. Analyses were performed at 135 °C with 1,2,4-trichlorobenzene as the solvent at 1.0 mL/min. The weight-average molecular weights and molecular weight distributions are shown in Table 1.

Films were obtained via compression molding in a Collin press between hot plates (160 °C for the homopolymer and 140 and 120 °C for the copolymers with low and high comonomer contents, respectively, to keep constant the difference between their melting points and the temperature of the hot plates) at a pressure of 2 MPa for 4 min. Two different thermal treatments were analyzed. The first thermal history, labeled S, consisted of a slow cooling (ca. 2 °C/min) from the molten state down to room temperature, at the inherent rate of the press, after the power was switched off. The second one, named Q, applied a fast quench (ca. 60 °C/min) between plates refrigerated with cold water after the melting of the material in the press.

Table 1. NMR and GPC Characterization

Sample	1-Hexene (mol %)	$M_w \times 10^{-3}$ (g/mol)[a]	M_w/M_n[b]	Tacticity
PP1	0.0	63	2.0	83.0
CPH2.1	2.1	69	2.1	85.8
CPH5.5	5.5	67	2.0	85.0

[a] Weight-average molecular weight.
[b] Weight-average molecular weight/number-average molecular weight.

Density determinations were performed at room temperature in a water–ethanol gradient column calibrated with glass floats. The gradient of the densities varied between 0.870 and 0.915 g/cm^3. The degree of crystallinity obtained from density measurements ($f_c^{density}$) was calculated with the following equation:[27,28]

$$f_c^{density} = (\rho_c/\rho)(\rho - \rho_a)/(\rho_c - \rho_a) \qquad (1)$$

Equation 1 is based on the assumption of a two-phase system, crystalline and amorphous, where ρ is the measured density of the sample and ρ_a and ρ_c are the densities of the completely amorphous and pure crystalline phases, respectively. The values of $\rho_a = 0.852$ g/cm^3 and $\rho_c = 0.936$ g/cm^3 for the amorphous and crystalline phase densities, respectively, were used.[29,30]

Wide-angle X-ray scattering (WAXS) patterns were recorded in the reflection mode, at room temperature, with a Philips diffractometer with a Geiger counter connected to a computer. Ni-filtered Cu Kα radiation was used. The diffraction scans were collected over a period of 20 min in the 2θ range of 3–43°, with a sampling rate of 1 Hz. The goniometer was calibrated with a silicon standard. The X-ray determinations of the degree of crystallinity were performed by subtraction of the corresponding amorphous component[31] in comparison with the totally amorphous profile of an elastomeric PP sample.

The thermal transitions were also investigated with real-time X-ray diffraction experiments with synchrotron radiation. These experiments were performed at the polymer beam line at Hasylab (Deutsches Elektronen Synchrotron (DESY), Hamburg, Germany). The beam was monochromatized (wavelength = 0.150 nm) by Bragg reflection through a germanium single crystal. Two linear position-sensitive detectors were used simultaneously, one of them covering the approximate 2θ range of 10–30° and the other being set at a sample–detector distance (in the direction of the beam) of 235 cm, covering a spacing range of 5–55 nm. Therefore, simultaneous WAXS and small-angle X-ray scattering (SAXS) data were collected.

Film samples of about 20 mg were covered with aluminum foil to ensure homogeneous heating or cooling and were placed in the temperature controller of the line *in vacuo*. A scanning rate of 8 °C/min was used. The scattering patterns were collected in time frames of 15 s, so that we had a temperature resolution of 2 °C between frames. The calibration of the spacings for the detectors was performed as follows: the diffractions of a crystalline PET sample were used for the WAXS detector, and the different orders of the long spacing of a rat-tail cornea (65 nm) were used for the SAXS detector.

The thermal properties were analyzed in a PerkinElmer DSC-7 calorimeter connected to a cooling system and calibrated with different standards at a heating rate of 20 °C min^{-1}. The sample weight ranged from 6 to 9 mg. The samples were first heated from −50 to 180 °C at a heating rate of 20 °C min^{-1} and then cooled to −50 °C at the same rate. For crystallinity determinations, a value of 209 J/g was taken as the enthalpy of fusion of the perfect α modification of iPP.[28]

The viscoelastic properties were measured with a Polymer Laboratories MK II dynamic mechanical thermal analyzer working in a tensile mode. The temperature dependence of the storage modulus (E'), loss modulus (E''), and loss tangent (tan δ) was measured at 3, 10, 30, and 50 Hz over a temperature range of −150 to 150 °C (this last temperature was modified according to the comonomer content) at a heating rate of 1.5 °C min^{-1}. The specimens were rectangular strips 2.2 mm wide, approximately 0.2 mm thick, and more than 15 mm long. The apparent activation energy values were calculated according to an Arrhenius-type equation, with an accuracy of ±0.5 °C in the temperature assignment of tan δ. The frequency dependence with the temperature in the relaxation mechanisms associated with the glass transition has also been considered to follow an Arrhenius behavior, although it is due to cooperative motions.[32] This approximation can be made without a significant error because the range of analyzed frequencies is low enough to be fitted to a linear behavior such as that just mentioned.

A Vickers indenter attached to a Leitz MH tester was used to carry out microindentation measurements. Experiments were undertaken at room temperature (23 °C). A contact load of 0.98 N and a contact time of 25 s were employed. MH values (MPa) were calculated according to the following relationship:[33]

$$MH = 2 \sin 68^{o} (P/d^2) \quad (2)$$

where P (N) is the contact load and d (mm) is the diagonal length of the projected indentation area.

RESULTS AND DISCUSSION

Structural and Thermal Characterization

Table 1 shows the main characteristics of the synthesized copolymers. They have similar molecular weights, polydispersities, and tacticities. Therefore, it will be considered in the following that these variables are not relevant for the discussion of the changes in the different properties of the samples. On the contrary, the density values, crystallinity, and thermal and mechanical properties depend considerably on the comonomer content, as discussed later.

The degree of crystallinity obtained from density measurements with eq 1 is shown in Table 2. The density and, therefore, crystallinity values decrease with increasing 1-hexene in the copolymers. On the other hand, the slowly cooled samples present higher density values than those quenched. At first approximation, this feature might indicate that a more perfect crystal structure is attained in the former specimens.

Figure 1 shows the WAXS traces of iPP and two copolymers either quenched (top plot) or slowly cooled (bottom plot) from the melt. The Q samples exhibit exclusively the characteristic diffractions of the α-monoclinic cell, whose diffraction peaks appear at 2θ values of 14.1, 16.9, 18.4, 21.1, and 25.8° corresponding to the (110), (040), (130), (111), and (041, 131) reflections of the α

Table 2. Density, Overall Degree of Crystallinity Obtained by Density ($f_c^{density}$) and WAXS (f_c^{WAXS}), Long Spacing (L), and Most Probable Crystal Size (l_c)

Sample	Density	$f_c^{density}$	f_c^{WAXS}	L (nm)	l_c (nm)
iPPQ	0.899	0.59	0.55	9.71	5.34
CPH2.1Q	0.894	0.52	0.40	8.80	3.55
CPH5.5Q	0.878	0.33	0.25	8.70	2.18
iPPS	0.904	0.64	0.58	11.36	6.59
CPH2.1S	0.895	0.54	0.50	10.75	5.38
CPH5.5S	0.883	0.40	0.42	10.53	4.42

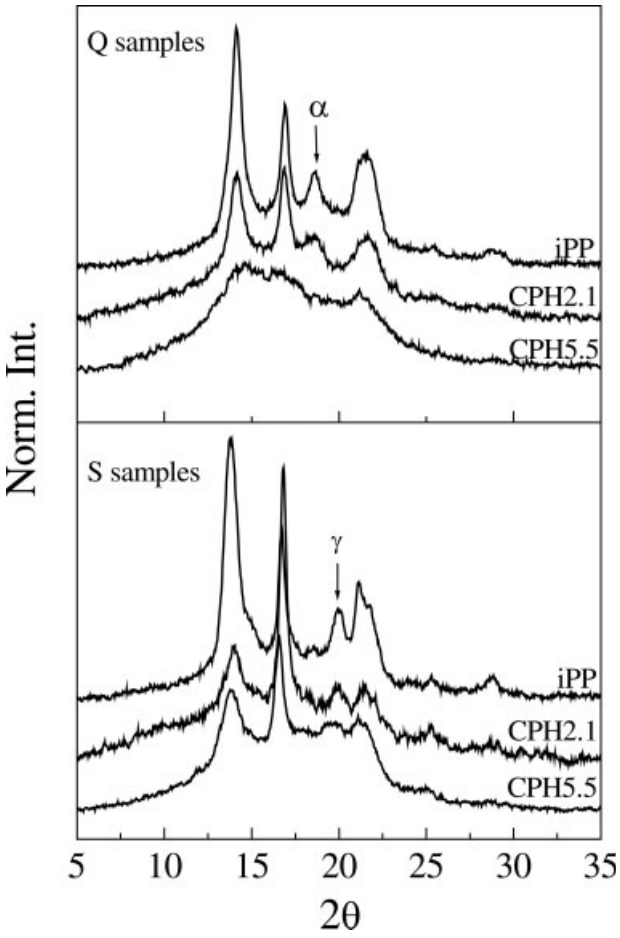

Figure 1. X-ray diffraction patterns, at room temperature, of different samples for the two thermal treatments.

modification of iPP.[34] The intensity of the different diffractions decreases as the comonomer content increases in the copolymer, and consequently, the crystallinity exhibits the same tendency. In addition, diffractions are broadened and shifted to lower angles; this indicates smaller and less perfect crystallites as the comonomer content is raised.

The diffraction profile corresponding to the quenched specimen of CPH5.5 shows rather diffuse diffraction peaks. In fact, only two wide maxima, centered around 15 and 21°, can be observed. A quite similar profile can be observed for the mesomorphic modification of iPP developed in efficiently quenched samples of this polymer.[35,36] It seems, therefore, that specimen CPH5.5Q is composed mainly of mesomorphic entities, although a certain amount of coexisting monoclinic crystallites cannot be disregarded.

This intermediate-ordered mesomorphic structure has also been found in copolymers of isotactic propylene and 1-octadecene with a molar fraction of approximately 5 and higher[14] under moderate quenching conditions. Therefore, it seems that the presence of the comonomer in the propene copolymers increases the ability to produce the mesomorphic modification because it is observed even under rather mild quenching conditions.

The iPP subjected to a slow crystallization process presents a well-defined peak at 19.9° corresponding to the (117) reflection,[37] which is characteristic of the γ modification. However, this diffraction is quite subtle in CPH2.1-S and almost imperceptible in the CPH5.5-S copolymer. The determination of the relative proportion of both phases is not straightforward because the diffractograms corresponding to the α and γ forms of iPP are rather similar. Therefore, several methods have been proposed.[25,38] A deconvolution procedure, after subtraction of the amorphous component,[23] has been used in this investigation. For that purpose, the amorphous halo of an elastomeric PP sample[31] has been used. The estimation of the X-ray crystallinity is now straightforward because all the original diffractograms are normalized to the same total intensity. Subsequently, the crystalline diffractograms are deconvoluted with Pearson VII profiles for the crystalline diffractions. The proportions of the two modifications are obtained from the relative areas of the diffractions at 2θ values of 18.5 and 19.9°. The results evidently undergo a slight change with a different method or different profiles for the fitting because of the diffraction overlapping. Moreover, it is assumed with this procedure that, in the samples with 100% α or γ modification, the relative areas of the diffractions at 18.5 and 19.9°, respectively, in relation to the total crystalline area, are the same in both cases. With this procedure, from the total crystallinity degree of 0.58 exhibited by sample iPPS, approximately 85% corresponds to the γ modification, and 15% corresponds to the α polymorph. A quantitative determination has not been performed for the copolymers because the error that can be accomplished is quite significant.

It has been reported in the literature that the development of the γ form is due to the interruptions in the PP isotactic sequences. These interruptions enclose either regio- or stereodefects and, in the copolymers, the comonomer units. Therefore, when discontinuities are more frequent, that is, at high comonomer contents, a high proportion of the γ polymorph is developed.[24,25,39] In this research, a conclusion involving the content of γ

modification with the comonomer molar fraction cannot be attained, as previously mentioned. This might be due to differences in the protocol of specimen preparation. Isothermal crystallization[39] at different temperatures and a much lower crystallization rate[25] (6 °C/h) have been used in comparison with the slow cooling rate (2 °C/min) here imposed.

A comparison of X-ray profiles of the quenched specimens and those slowly cooled points out the smaller crystallinity developed in the former samples, the differences being more important as the comonomer content increases, as can be deduced from the values shown in Table 2. Moreover, the better resolved diffractograms suggest better ordering and longer crystallites in the slowly cooled specimens. These features have been confirmed by the estimation of the size of the ordered entities by SAXS. The corresponding long spacings are presented in Table 2, showing significantly higher values for the S specimens. From these values and the total WAXS crystallinity of the sample, the most probable crystallite size in the direction normal to the lamellae can be estimated by the assumption of a simple two-phase model. The results for the most probable crystallite size are also listed in Table 2. The crystallites become smaller as the crystallization rate is raised during cooling because quenching limits the development and perfection of the crystalline entities. However, it is evident that the comonomer content is the most important variable determining the crystalline morphology (crystallinity and crystal size), as expected, because the lateral branches of 1-hexene are long enough to be excluded from the crystalline cell of iPP.[39]

Figure 2 illustrates the thermal behavior of the different samples during the first melting after processing to analyze the crystalline structure that directly affects the mechanical properties. On the one hand, a displacement to lower glass-transition temperatures and melting temperatures is observed with increasing comonomer content. On the other hand, a clear annealing peak is exhibited for the different samples, especially for the copolymer with the highest comonomer content, CPH5.5. There is an important fraction of the sample that has crystallized during processing into rather small and imperfect crystallites, primarily within the quenched specimens. Therefore, they are able to melt and recrystallize during the stay of samples at room temperature before their analysis. These initially small crystallites are slightly enlarged, leading to the appearance of that

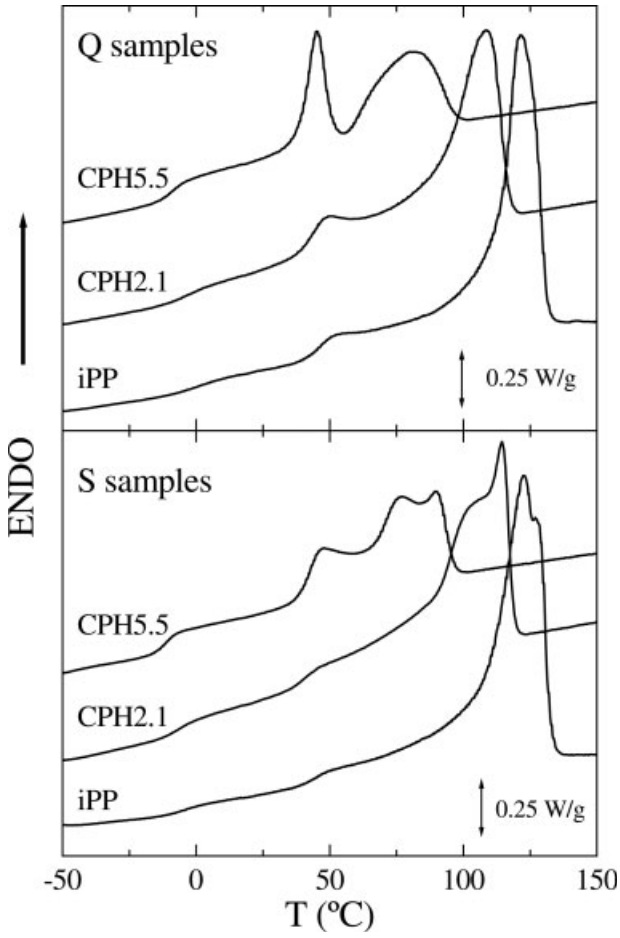

Figure 2. DSC first melting curves for the homopolymer and copolymers with both thermal histories at 20 °C/min.

peak located at 40–50 °C. This feature is important on account of the influence of annealing on the mechanical response[27] because this stay at room temperature for a few days leads to an improvement in the crystalline regions, increasing the crystal perfection and crystallinity, as observed by a comparison of the degrees of crystallinity obtained from differential scanning calorimetry (DSC) during the first and second heating processes (Table 3).

Moreover, the melting enthalpy is also significantly reduced when the 1-hexene content increases in the copolymer. The introduction of more comonomer units hinders the chain regularity needed for the crystallization process. Consequently, the crystallinity degree of the copolymers, estimated from the melting endotherm, is lowered as the 1-hexene content increases (see Table 3).

The slowly cooled samples present glass-transition temperatures lower than those found for

Table 3. Glass-Transition Temperature (T_g), Melting Temperature (T_m), and Degree of Crystallinity Obtained by DSC (f_c^{DSC}) for the First and Second Melting and Crystallization Temperature (T_c)[a]

Sample	$T_{g,1}$ (°C)	$T_{m,1}$ (°C)	$T_{g,2}$ (°C)	$T_{m,2}$ (°C)	$f_{c,1}^{DSC}$	$f_{c,2}^{DSC}$	T_c (°C)
iPPQ	1	122	−6	123	0.43	0.39	83
CPH2.1Q	−1	109	−8	108	0.34	0.28	65
CPH5.5Q	−9	80	−14	81	0.17	0.16	0
iPPS	−3	123, 127	—	—	0.46	—	—
CPH2.1S	−5	107, 114	—	—	0.35	—	—
CPH5.5S	−12	77, 90	—	—	0.23	—	—

[a] Subscripts 1 and 2 represent the first and second melting, respectively.

the Q samples (Table 3). This effect can be attributed to the existence of two types of crystallites: those organized into an α lattice and those with a γ arrangement, as confirmed by the X-ray results. The γ structure is composed of smaller and thinner crystals in comparison with those of the α modification. These thinner crystallites seem to lead to a lower movement restriction within the amorphous phase.

Another characteristic, shown in Figure 2, is the splitting of the main melting peak found in the slowly cooled samples, most likely due to the just mentioned coexistence of the γ and α crystallites and thus their corresponding melt processes. The melting that takes place at low temperatures is related to the γ phase, whereas the one associated with the α modification occurs at a slightly higher temperature.[39] The two melting temperatures have been estimated by deconvolution of the melting curve at that temperature interval, and their values are listed in Table 3. Although the γ crystallites are formed at higher temperatures, they are less stable than the monoclinic ones and melt at lower temperatures.[39]

Figure 3 shows the second melting process for iPP and the two copolymers. The most important feature is the appearance of a cold crystallization in CPH5.5 because this sample does not crystallize totally during the cooling process at 20 °C/min. It is also evident from this figure that there is no annealing peak in the second melting of the three samples, as expected. Moreover, the main melting endotherms do not present appreciable splitting because at this relatively fast crystallization rate (cooling at 20 °C/min), the proportion of the γ phase formed is rather low (if any).

As commented previously, copolymer CPH5.5 does not crystallize completely during the cooling at 20 °C/min. A more detailed analysis of the crystallization behavior of this copolymer has been performed via cooling from the melt at different rates. Figure 4 shows the melting curves after cooling from the melt at the indicated rates. First, the cold crystallization, which appears around 10 °C, diminishes in intensity as the cooling rate does in such a way that the specimen cooled at 5 °C/min does not present appreciable cold crystallization. Moreover, the effect of the extent of crystallization on the glass-transition temperature is rather evident: it passes from −18 °C for the sample cooled at 40 °C/min to −10 °C for the one totally crystallized during the cooling process (at 5 °C/min). Additionally, at the

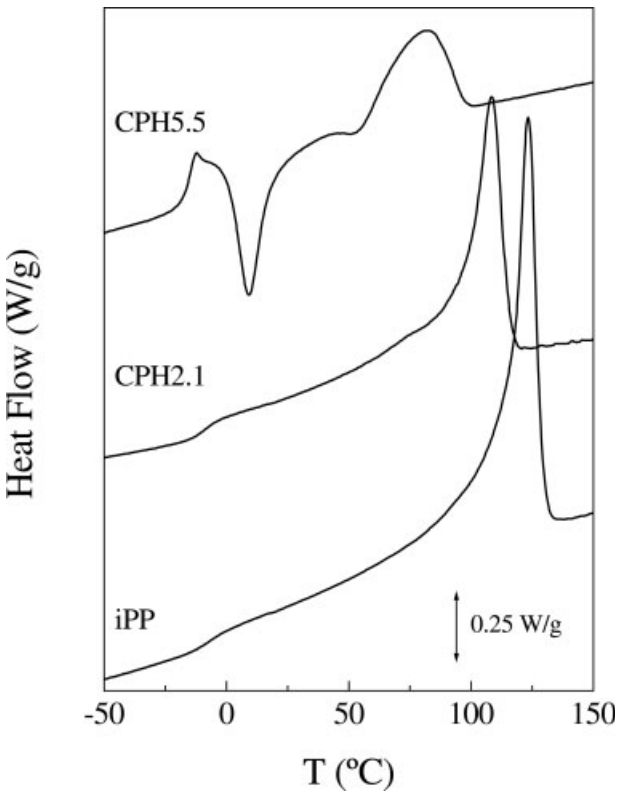

Figure 3. DSC second melting curves for the homopolymer and copolymers crystallized at 20 °C/min

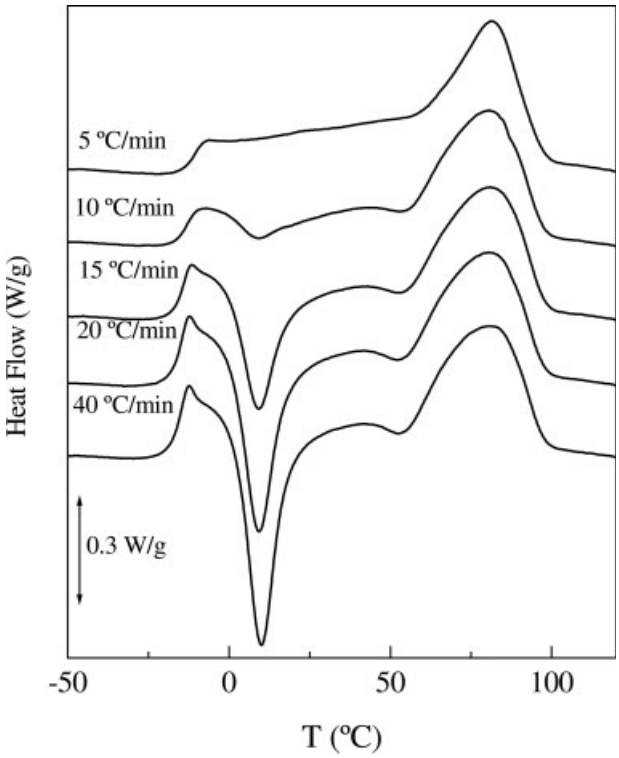

Figure 4. DSC melting curves for the CPH5.5 copolymer after crystallization at different rates: 5, 10, 15, 20, and 40 °C/min (from top to bottom).

glass transition, the difference in the specific heat between the glassy and rubbery states increases with the crystallization rate (see Fig. 4), pointing out the progressive decrease in the crystallinity.

Synchrotron Measurements

In addition to the previous analysis of the long spacing for all the samples at room temperature (see results in Table 2), the slowly cooled specimens were also investigated by real-time variable-temperature experiments employing synchrotron radiation. Simultaneous SAXS/WAXS profiles were acquired during the heating of the samples at 8 °C/min. The diffraction profiles corresponding to samples iPPS and CPH5.5S are shown in Figures 5 and 6, respectively.

Regarding the WAXS diffractograms, they have a poorer resolution than those presented in Figure 1, so now the determination of the relative proportions of the α and γ modifications is even more difficult. It is clear, however, that in the three S-type specimens, the γ modification is predominant.

The SAXS results appear to be more interesting. The values of the most probable long spacing, deduced from the Lorentz-corrected SAXS profiles, are shown in Figure 7 as a function of temperature. Focusing our attention on sample iPPS, we can observe three regions: an initial one, up to around 60 °C, in which the long spacing is almost constant; a second region, between 60 and approximately 105 °C, with a moderate increase in the long spacing; and a final one, with a very important thickening. This last region coincides with the main melting endotherm (see Fig. 2) and is ascribed to the usual melting–recrystallization phenomena. On the other hand, the end of the first region (and the beginning of the second) is approximately the temperature at which the annealing peak is observed.

In the case of sample CPH2.1S, the results are rather similar, with some minor differences: the initial long spacings are somewhat lower than those for iPPS, and the final thickening region occurs at lower temperatures, corresponding to lower melting temperatures.

The behavior for sample CPH5.5S is, however, quite different because now the second and third regions mentioned previously seem to be coincident, and the thickening is much smaller.

Nevertheless, the values of the long spacing are very similar for the three samples in the first two regions. However, the crystal thickness, deduced from the long spacing and the overall crystallinity, decreases considerably from iPP to CPH5.5 (see Table 2 for the room-temperature values).

Additional information can be obtained from the analysis of the relative SAXS invariant.[40–42] The temperature evolution of this invariant for the three S-specimens is shown in the upper part of Figure 8. After an initial region of a very small increase in the invariant, it follows a more considerable increase, before the final sharp decrease during melting.

The lower part of Figure 8 shows the corresponding derivatives of the relative invariant. These derivatives are rather similar to the melting endotherms (see Fig. 2), although the peaks are now smoother than the DSC curves. The reason may be either the much lower temperature resolution of the synchrotron experiments (the diffraction profiles are the averages of every 15 s, the time frame) or a much smaller sensitivity of these SAXS results to the presence of α and γ crystals. Anyway, the overall temperature profiles of the synchrotron and DSC results are remarkably similar.

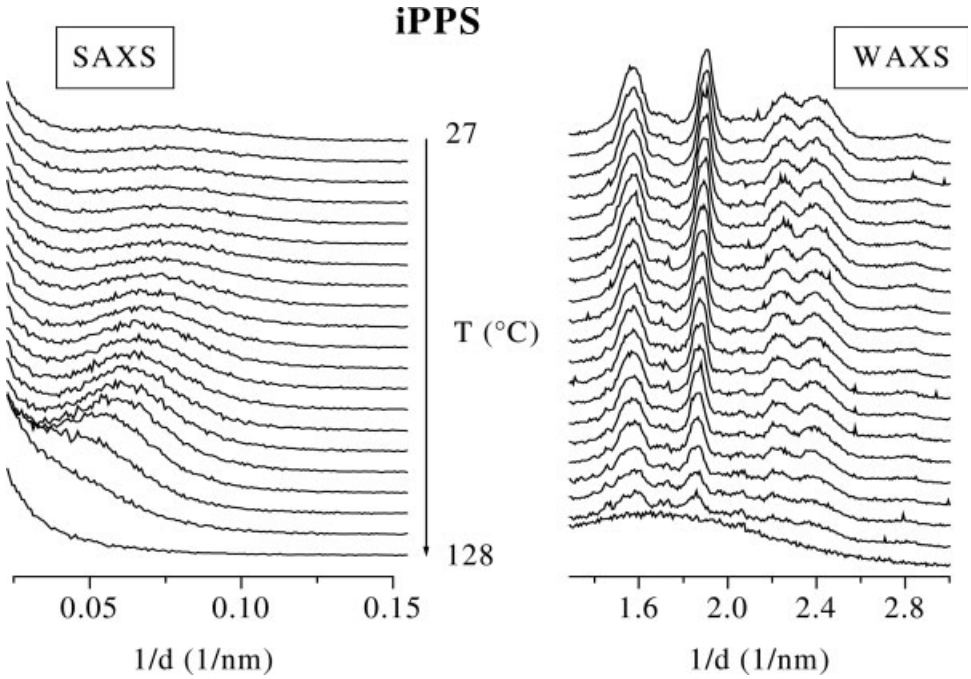

Figure 5. Real-time SAXS and WAXS profiles, obtained with synchrotron radiation for iPPS, for a melting experiment at 8 °C/min. Only one of every two frames is plotted for clarity.

Dynamic Mechanical Properties

Figure 9 shows plots of E', E'', and tan δ as functions of temperature for the different specimens. The viscoelastic behavior of iPP and the copolymers is influenced by variables that affect the crystalline structure,[14] such as the comonomer content, degree of crystallinity, thermal treatment, and, therefore, γ-form content in the specimens synthesized with metallocene catalysts. iPP obtained with Ziegler–Natta catalysts (iPP)

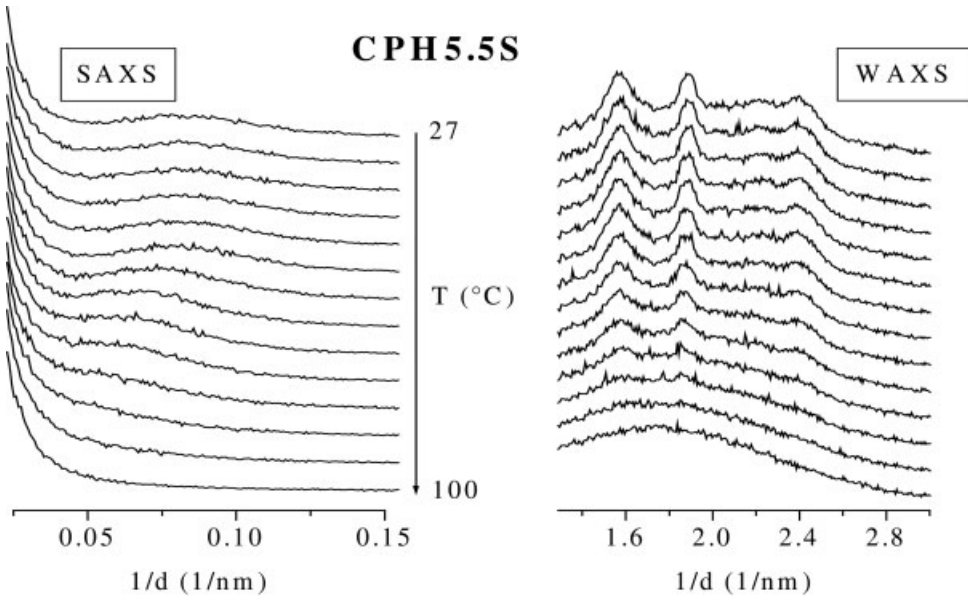

Figure 6. Real-time SAXS and WAXS profiles, obtained with synchrotron radiation for CPH2.1S, for a melting experiment at 8 °C/min. Only one of every two frames is plotted for clarity.

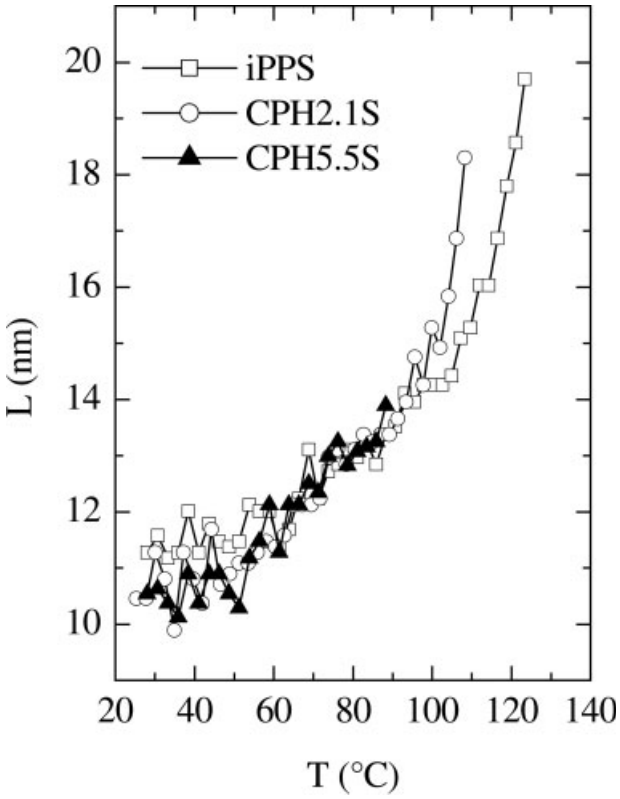

Figure 7. Effect of the temperature (T) on the Lorentz-corrected long spacing (L) for different S-specimens during the melting experiments.

as well as metallocene PP presents three viscoelastic relaxations,[32,43] as depicted in Figure 9. The γ relaxation is due to the rotation of methyl groups, centered around -55 °C; the β process is associated with the glass transition of the amorphous regions, at about 0 °C; and the third relaxation, named α, is related to movements involving the crystalline phase.

The structural parameters (mainly the comonomer content, crystallinity, and crystal size) do influence the location and intensity of the different relaxation processes. Looking at the tan δ plot, we can clearly observe the α mechanism only in iPP for both treatments and in CPH2.1S. However, it appears for all the different specimens analyzed in the high-temperature side of the β process as a shoulder in E'' graphs and as a significant drop in the E' plots at temperatures higher than that associated with the glass transition. From these plots and Table 4, a shift to lower temperatures is found in the location of the α process as the comonomer content increases. The crystallites become smaller and their number is diminished with the 1-hexene content (Table 2), and consequently, their motions can start at lower temperatures.

On the other hand, the β relaxation (associated with the glass-transition temperature) is also dependent on the 1-hexene composition. The motions in this case take place within the amorphous regions, whose content increases with the 1-hexene molar fraction. Additionally, all the details related to improvements in crystallites (crystallinity, perfection, and size) hinder this movement. Therefore, its intensity becomes significantly higher and its location is moved to lower temperatures as comonomer incorporation is raised in the copolymers (see Fig. 9 and Table 4). Concerning the effect of the thermal treatment, it seems that the presence of γ crystallites in the slowly cooled specimens reduces the hindrance to motion within the amorphous regions, probably because of their lower size in comparison with that presented by α crystallites. Thus, the location of this relaxation is found at a lower temperature in the S

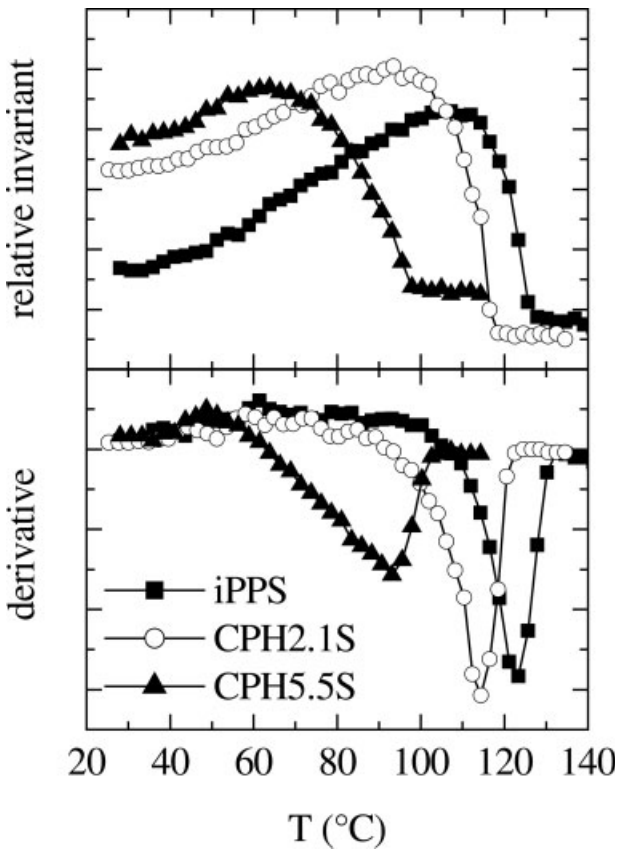

Figure 8. Temperature (T) dependence of the relative SAXS invariants (top) and SAXS invariant derivative (bottom) for different S-specimens during the melting experiments.

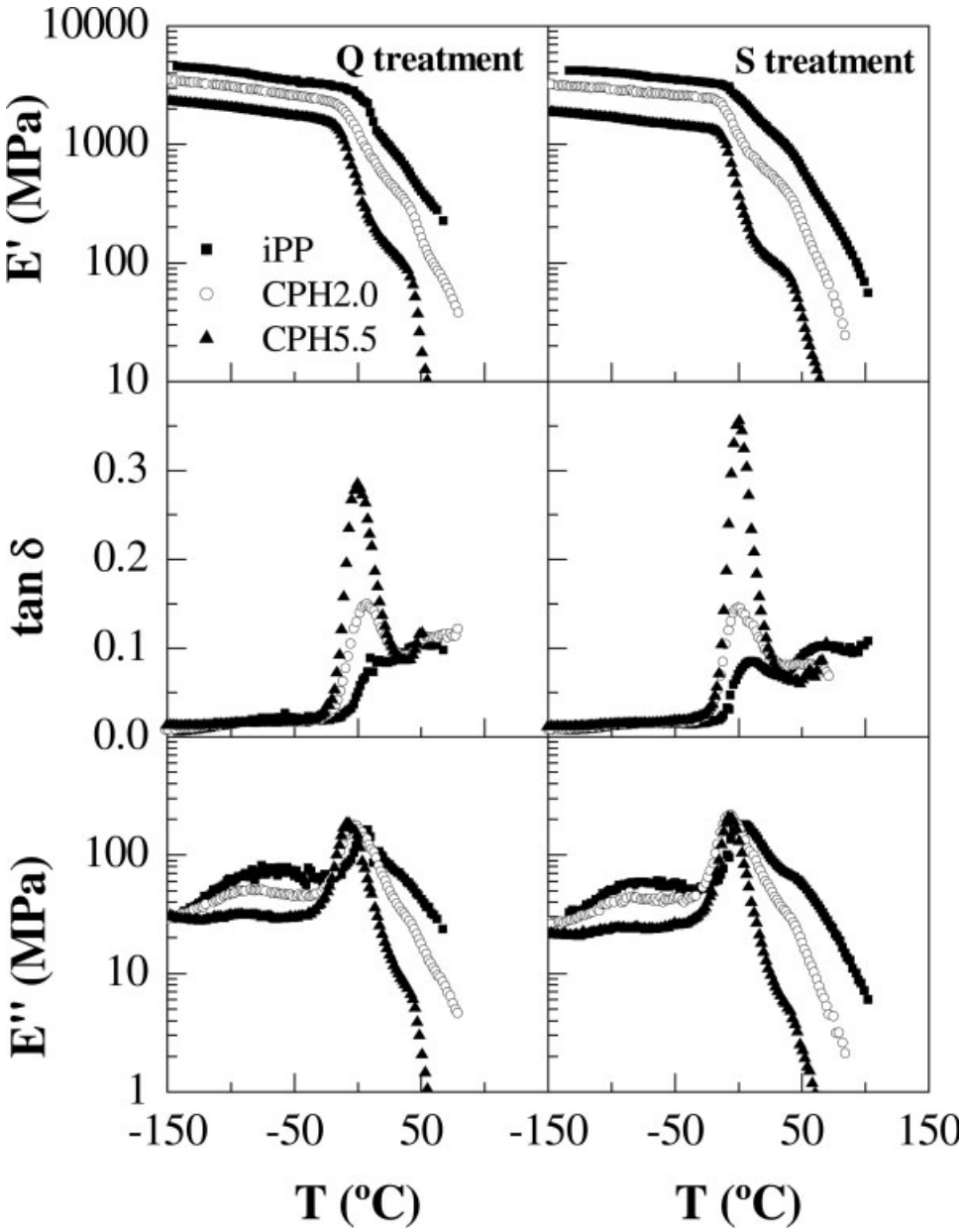

Figure 9. Temperature (T) dependence of the real and imaginary components of the complex modulus and tan δ of different samples.

samples at a given composition, similarly to the DSC results. In CPH5.5, this thermal history influence is minimized because the Q specimen is practically mesomorphic instead of being arranged into α crystallites.

The γ relaxation of PP is observed for all the copolymers. Its intensity is considerably reduced and its position is shifted to lower temperatures as the 1-hexene content increases in the specimens (see Fig. 9 and Table 4). These features might be related to a decrease in the steric effect between the methylene groups pendant from the PP backbone responsible for this motion.

Mechanical Response

E′

Figure 9 also shows the effect of the comonomer content for both thermal treatments on the elastic component of the complex modulus at 3 Hz. A considerable decrease in E' can be observed as the 1-hexene content increases because of a re-

Table 4. Temperatures (Tan δ Basis, 3 Hz) and Apparent Activation Energies (kJ/mol) of the Dynamic Mechanical Relaxations

Sample	T_γ	T_β	T_α	E_a^γ	E_a^β	E_a^α
iPPQ	−61.0	11.0	54.0	70	350	150
CPH2.1Q	−73.0	5.5	—	65	320	—
CPH5.5Q	−78.5	0.5	—	55	290	—
iPPS	−67.5	10.5	68.0	70	350	150
CPH2.1S	−78.0	1.0	46.0	60	310	—
CPH5.5S	−80.0	0.5	—	50	270	—

duction in the stiffness. This loss of rigidity observed in the copolymers can be ascribed to the diminishment of the crystallinity and crystallite thickness. This rigidity reduction is more important at high temperatures, above the glass transition. The E' values at room temperature are listed in Table 4.

On the other hand, the effect of the thermal treatment applied during processing is practically negligible at subambient temperatures for a given specimen. However, above the β relaxation associated with cooperative motion within the amorphous regions, slowly cooled specimens exhibit slightly higher E' values than samples quenched from the melt, probably because of their higher overall crystallinity (see Table 5).

MH Measurements

MH is another significant mechanical magnitude in polymers, measuring the resistance of the material to plastic deformation, and accordingly provides an idea about local strain. MH involves a complex combination of properties (the elastic modulus, yield strength, strain hardening, and toughness). Its dependence on the comonomer content and thermal treatment is quite analogous to that observed for E' in the copolymers under study, as depicted in Figure 10 and detailed in Table 5. Therefore, a direct relationship is commonly found between the elastic modulus and MH,[32] and the following empirical equation has been proposed:

$$\mathrm{MH} = aE^b \tag{3}$$

where a and b are constants and E is the elastic modulus. This equation is also fulfilled by many systems,[27,44,45] from thermoplastic elastomers to very rigid polymers, that is, in a very broad range of MH and E values. Figure 11 shows a good linear relationship between MH and E' in the different specimens analyzed for the two thermal treatments.

Impact Strength

Because of the practical importance of improving the impact resistance of iPP, the impact strength of the studied samples has been estimated by the consideration of such a magnitude related to the area of the tan δ curves. The correlation of the impact resistance with dynamic mechanical behavior has been indicated by many authors.[3,46–49] The area under the tan δ curve from −150 to 30 °C provides an estimation of the impact strength, although it is not a direct measurement. A linear correlation between the notched Izod impact strength and the area under tan δ has been observed for iPP/ethylene-vinyl acetate copolymer (EVA) blends,[48] whereas an exponential relationship has been found for the iPP/EPDM blends.[48] In the samples studied here, the incorporation of 1-hexene into iPP by copolymerization leads to an increase in such an area and, accordingly, enhances the insufficient impact resistance of PP at a low temperature, as shown in Table 5. Comparing these results with those shown by a commercial Ziegler–Natta

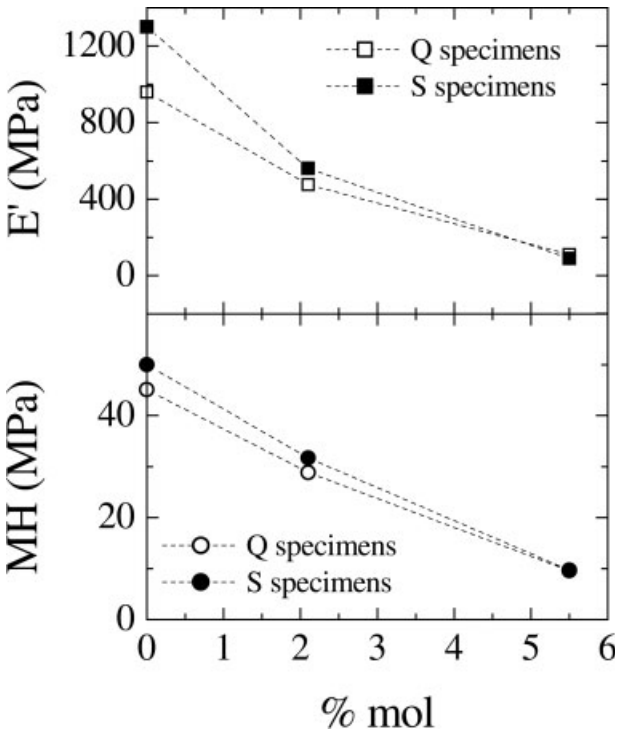

Figure 10. Variation of E' and MH as a function of the comonomer content.

iPP[49] and a commercial multiphasic PP,[3] both toughened with a plastomer, we find that the area under the tan δ curve in these copolymers shows a larger increase than that observed in the case of the aforementioned blends. The areas for the iPP/plastomer and heterophasic iPP/plastomer, both with 25 wt % plastomer, are 4.5 and 5.9, respectively, taking into account that the area for the iPP homopolymer is 3.5 and that for heterophasic iPP is 4.0. Therefore, on the one hand, the metallocene iPP now analyzed presents an enhanced impact strength with respect to that exhibited by the other two iPPs synthesized with Ziegler–Natta catalysts, probably because of the smaller crystallites that developed in the former specimen. On the other hand, the incorporation of the comonomer seems to be more effective than blending because the areas are much higher and the weight percentages are 4.1 and 10.4 in CPH2.1 and CPH5.5, respectively, values considerably lower than the value of 25 wt % previously mentioned for the plastomer.

However, such an impact-strength improvement is accompanied by a considerably higher decrease in rigidity and then in the modulus for the copolymers in comparison with the blends. Therefore, the choice of one polymeric material type or another (copolymers or blends) has to be taken as a function of the best compromise between rigidity and toughness necessary to accomplish the final requirements for a specific application. The metallocene block copolymers with soft and hard domains[10–13] synthesized with rubbery polyolefin macromonomers might also be a very interesting approach.

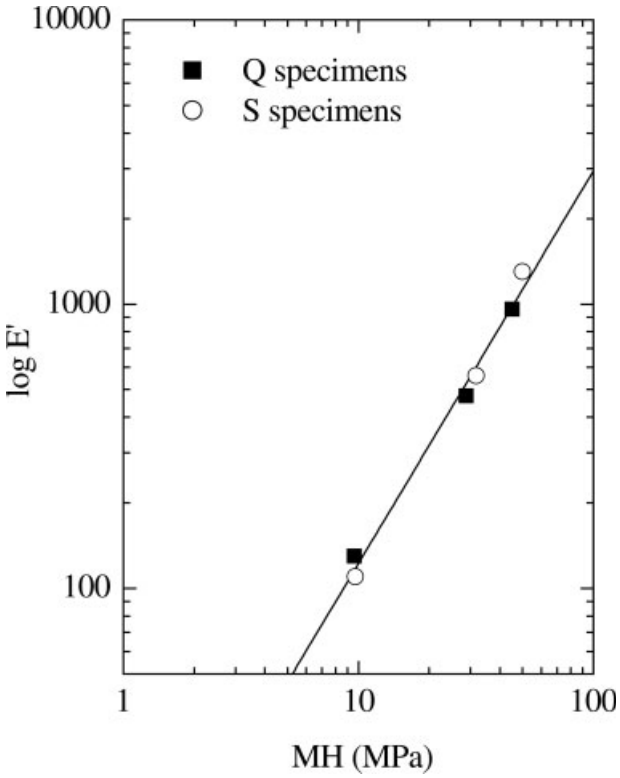

Figure 11. Relationship between MH and E' in different samples.

Table 5. E' and MH at Room Temperature and Area under the Tan δ Curve from −150 to 30°C.

Sample	E' (MPa)	MH (MPa)	Area under the Tan δ Curve (Arbitrary Units)
iPPQ	960	45.1	5.0
CPH2.1Q	480	28.8	7.5
CPH5.5Q	90	9.6	10.9
iPPS	1300	50.0	4.8
CPH2.1S	560	31.7	7.3
CPH5.5S	110	9.7	11.7

CONCLUSIONS

From the structural, thermal, and mechanical characterization of two copolymers of propylene and 1-hexene (and of the corresponding homopolymer) synthesized by an isotactic metallocene catalyst, the relationships between the structure and properties have been established.

The most important factor affecting the structure and properties of these copolymers is the comonomer content. The thermal treatment, that is, the rate of cooling from the melt, is also important. These factors affect the thermal properties, the degree of crystallinity, and therefore the structural parameters and the viscoelastic behavior. A slow cooling from the melt favors the formation of the γ phase instead of the α modification.

On the other hand, the β relaxation, associated with the glass-transition temperature, is shifted to lower temperatures, and its intensity is increased as the 1-hexene content raises. The MH values are correlated with those of E' deduced from dynamic mechanical thermal analysis curves, and good linear relations have been obtained between these parameters. The indirect estimation of the impact strength has shown that area values in the CPH copolymers are higher than those observed in some reported blends

with plastomers, although copolymerization leads to a stronger drop in the modulus.

The authors are grateful for the financial support of the Comunidad Autónoma de Madrid, Ministerio de Educación y Ciencia, CONICYT, and CONICYT/Consejo Superior de Investigaciones Científicas Exchange Collaboration Program (project 07N/0093/2002, project MAT2004-01547, project FONDAP 11980002 and scholarship to H. Palza, and project 2003CL0028, respectively). Support from the European Commission (COST Action D17, WG D17/0004/00) is also acknowledged. J. M. López-Majada is grateful to Repsol-YPF for its financial support. Additionally, the authors thank G. B. Galland (Instituto de Quimica, Universidade Federal do Rio Grande do Sul, Porto Alegre, Brazil) for help with the NMR measurements and discussion. The synchrotron work (in the A2 polymer line of Hasylab at DESY, Hamburg, Germany) was supported by the European Community Research Infrastructure Action under the FP6 "Structuring the European Research Area" Program (through the Integrated Infrastructure Initiative "Integrating Activity on Synchrotron and Free Electron Laser Science", contract RII3-CT-2004-506008). The authors thank the Hasylab personnel, especially S. Funari, for their collaboration.

REFERENCES AND NOTES

1. Galli, P.; Vecellio, G. J Polym Sci Part A: Polym Chem 2004, 42, 396.
2. Galli, P.; Vecellio, G. Prog Polym Sci 2001, 26, 1287.
3. Arranz-Andrés, J.; Benavente, R.; Peña, B.; Pérez, E.; Cerrada, M. L. J Polym Sci Part B: Polym Phys 2002, 40, 1869.
4. Arranz-Andrés, J.; Benavente, R.; Pérez, E.; Cerrada, M. L. Polym J 2003, 35, 766.
5. Sinn, H.; Kaminsky, W. Adv Organomet Chem 1980, 18, 99.
6. Sinn, H.; Kaminsky, W.; Vollmer, H. J.; Woldt, R. Angew Chem 1980, 19, 390.
7. Kaminsky, W.; Laban, A. Appl Catal A 2001, 222, 47.
8. Ewen, J. A.; Jones, R. L.; Razavi, A.; Ferrara, J. D. J Am Chem Soc 1988, 110, 6255.
9. (a) Brintzinger, H. H.; Fischer, D.; Mulhaupt, R.; Rieger, B.; Waymouth, R. M. Angew Chem 1995, 107, 1255; (b) Brintzinger, H. H.; Fischer, D.; Mulhaupt, R.; Rieger, B.; Waymouth, R. M. Angew Chem Int Ed Engl 1995, 34, 1143.
10. Shiono, T.; Azad, S. M.; Ikeda, T. Macromolecules 1999, 32, 5723.
11. Weng, W.; Markel, E. J.; Dekmezian, A. H. Macromol Rapid Commun 2001, 22, 1488.
12. Kolodka, E.; Wang, W.-J.; Zhu, S.; Hamielec, A. E. Macromol Rapid Commun 2002, 23, 470.
13. Kolodka, E.; Wang, W.-J.; Zhu, S.; Hamielec, A. E. Macromolecules 2002, 35, 10062.
14. Palza, H.; López-Majada, J. M.; Quijada, R.; Benavente, R.; Pérez, E.; Cerrada, M. L. Macromol Chem Phys 2005, 206, 1221.
15. Quijada, R.; Guevara, J. L.; Galland, G. B.; Rabagliati, F. M.; Lopez-Majada, J. M. Polymer 2005, 46, 1567.
16. Poon, B.; Rogunova, M.; Hiltner, A.; Baer, E.; Chum, S. P.; Galeski, A.; Piorkowska, E. Macromolecules 2005, 38, 1232.
17. Marigo, A.; Marega, C.; Saini, R.; Camurati, I. J Appl Polym Sci 2001, 79, 375.
18. Lotz, B.; Graff, S.; Wittman, J. C. J Polym Sci Part B: Polym Phys 1986, 24, 2017.
19. Jones, A. T.; Aizlewood, J. M.; Beckett, D. R. Makromol Chem 1964, 75, 134.
20. Alamo, R. G.; Lucas, J. C.; Mandelkern, L. Polym Prepr 1994, 35, 406.
21. Natta, G.; Corradini, P. Nuovo Cimento Suppl 1960, 15, 40.
22. Thomann, R.; Wang, C.; Kressler, J.; Mülhaupt, R. Macromolecules 1996, 29, 8425.
23. Pérez, E.; Zucchi, D.; Sacchi, M. C.; Forlini, F.; Bello; A. Polymer 1999, 40, 675.
24. Guidetti, G. P.; Busi, P.; Giulianelli, I.; Zannetti, R. Eur Polym J 1983, 19, 757.
25. Turner-Jones, A. Polymer 1971, 12, 487.
26. Guevara, J. L. Ph.D. Thesis, University of Chile, 2004.
27. Benavente, R.; Pérez, E.; Quijada, R. J Polym Sci Part B: Polym Phys 2001, 39, 277.
28. Isasi, J. R.; Mandelkern, L.; Galante, M. J.; Alamo, R. G. J Polym Sci Part B: Polym Phys 1999, 37, 323.
29. Pérez, E.; Benavente, R.; Bello, A.; Pereña, J. M.; Zucchi, D.; Sacchi, M. C. Polymer 1997, 38, 5411.
30. Polymer Handbook, 4th ed.;Brandrup, J.;Immergut, J. D., Eds.;Wiley: New York, 1999.
31. Mansel, S.; Pérez, E.; Benavente, R.; Pereña, J. M.; Bello, A.; Röll, W.; Kirsten, R.; Beck, S.; Brintzinger, H.-H. Macromol Chem Phys 1999, 200, 1292.
32. McCrum, N. G.; Read, B. E.; Williams, G. Anelastic and Dielectric Effects in Solid Polymers; Dover: New York, 1991.
33. Baltá Calleja, F. J. Adv Polym Sci 1985, 66, 117.
34. Alizadeh, A.; Richardson, L.; Xu, J.; McCartney, S.; Marand, H.; Cheung, Y. W.; Chum, S. Macromolecules 1999, 32, 6221.
35. Androsch, R.; Wunderlich, B. Macromolecules 2001, 34, 5950.
36. Alexander, L. E. X-Ray Diffraction Methods in Polymer Science; Wiley-Interscience: New York, 1969.
37. De Rosa, C.; Auriemma, F.; Circelli, T. Macromolecules 2002, 35, 3622.
38. Rieger, B.; Mu, X.; Mallin, D. T.; Rausch, M. D.; Chien, J. C. W. Macromolecules 1990, 23, 3559.
39. Hosier, I. L.; Alamo, R. G.; Estero, P.; Isasi, J. R.; Mandelkern, L. Macromolecules 2003, 36, 5623.

40. Baltá-Calleja, F. J.; Vonk, C. G. X-Ray Scattering of Synthetic Polymers; Elsevier: Amsterdam, 1989.
41. Ryan, A. J.; Stanford, J. L.; Bras, W.; Nye, T. M. W. Polymer 1997, 38, 759.
42. Crist, B. J Polym Sci Part B: Polym Phys 2001, 39, 2454.
43. Jourdan, C.; Cavaille, J. Y.; Perez, J. J Polym Sci Part B: Polym Phys 1989, 27, 2361.
44. Cerrada, M. L.; de la Fuente, J. L.; Fernández-García, M.; Madruga, E. L. Polymer 2001, 42, 4647.
45. Lorenzo, V.; Pereña, J. M.; Fatou, J. M. Angew Makromol Chem 1989, 172, 25.
46. Heijboer, J. J Polym Sci 1967, 16, 3755.
47. Ramsteiner, F. Polymer 1979, 20, 839.
48. Jafari, S. H.; Gupta, A. K. J Appl Polym Sci 2000, 78, 962.
49. Prieto, O.; Pereña, J. M.; Benavente, R.; Pérez, E.; Cerrada, M. L. J Polym Sci Part B: Polym Phys 2003, 41, 1878.